Disponible en ligne sur
ScienceDirect
www.sciencedirect.com
Elsevier Masson France
EM|consulte
www.em-consulte.com
IRBM 38 (2017) 298–303
IRBM

RITS 2017

Local Orientation Imaging for Tissue Structure Using Ultrasound Imaging

E. Turquin *, L. Petrusca, O. Bernard, M. Viallon, H. Liebgott, F. Varray

Univ. Lyon, INSA–Lyon, Université Claude Bernard Lyon 1, UJM–Saint Etienne, CNRS, Inserm, CREATIS UMR 5220, U1206, F-69621, Lyon, France

Received 17 March 2017; received in revised form 27 July 2017; accepted 14 August 2017
Available online 5 September 2017

Highlights

- A method determining local anisotropic was studied.
- We are the second team to study this method.
- Results obtained with this method are very hopeful.

Graphical abstract

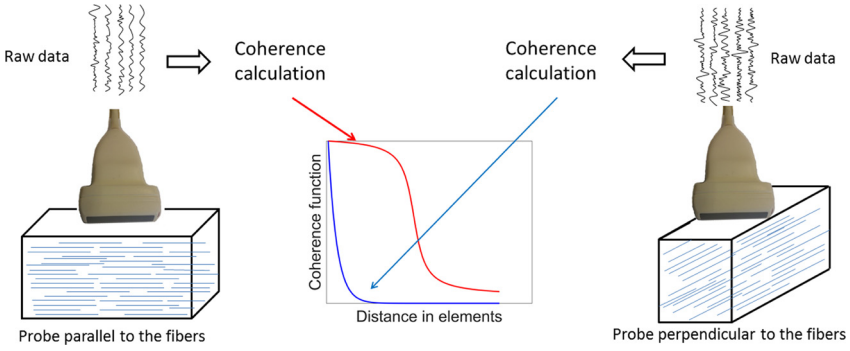

Abstract

Cardiovascular diseases and myocardium infarction are main causes of death worldwide. After acute myocardium infarction, remodeling occurs within weeks resulting from a loss of cardiomyocytes in the damaged myocardium, and subsequent changes with regional tissue organization. Imaging methods able to render the local tissue directivity would be useful to detect the lesion and evaluate its extent. In this field, diffusion MRI is the reference. However, because of its long acquisition time, it is not simple to make an image of the moving heart *in vivo*. For this reason, faster methods using ultrasound were developed. The purpose of this work is to study the spatial coherence method with an ultrasound plane wave ultrafast imaging approach. Simulations have been performed with CREANUIS software on a medium constituted by many angled fibers in order to mimic the orientation changes that appear in the myocardium. Experimental data were also acquired on a wires phantom. The wires of the phantom were set in parallel planes with changing orientation between [−45° and 45°] at a depth between [20 and 40 mm]. Results obtained with the method have permitted to evaluate properly the orientation with RMSE of 11.2° and 16.5° for simulation and experiments, respectively.

Keywords: Ultrasound; Heart; Fibers; Spatial coherence

1. Introduction

Cardiovascular disease remains the leading cause of death in adults and in industrialized countries (WHO, update 2014). Among them, ischemic heart disease is the main cause of death and hospitalization with infarct size being the major factor of prognosis after acute myocardial infarction (AMI). It is a main cause of heart failure. Interventions to reduce final infarct size thus have a major clinical interest in improving the prognosis of patients referred for myocardial infarction. The current management of myocardial infarction is to reperfuse the my-

* Corresponding author.
E-mail address: emeline.turquin@creatis.insa-lyon.fr (E. Turquin).

http://dx.doi.org/10.1016/j.irbm.2017.08.002

ocardium as soon as possible by primary percutaneous coronary intervention (PCI). The muscular cells in the heart tissue, the cardiomyocytes, are elongated. They are assembled in fibers which are elongated too. In the unfortunately unsaved myocardium, cell loss is irremediable leading to a progressive local disorganization and change in the tissue structure then functioning of the heart [1]. Cells are too small to be detected by ultrasounds but their organization in the myocardial tissue and so their orientation is very important and can be detected. An imaging method able to measure the local tissue organization, structure and directivity would be extremely useful to qualify and characterize the lesion. The purpose of this work is, thus to develop an ultrasound based imaging method that enables to determine the local tissue orientation in the heart and provide new solutions to enable advanced tissue characterization by ultrasound imaging.

Imaging of the fibers orientation can already be performed using diffusion MRI [2] which is the reference in this field. However, long acquisition time is still required (approximately 25 min in clinical cases), with motion of the organs being a main source of bias to circumvent prior quantitative estimates of the tissue structure could be obtained with the high reliability needed for clinical application. This is why, faster methods allowing to obtain images *in vivo* at high frame rate have to be developed: in this context ultrasound is an excellent candidate. Indeed, ultrasound allows imaging the heart at several tens of frames per second in conventional imaging and can even reach several thousand frames per second with high frame rate strategies. Only three methods have been developed previously to image tissue anisotropy based on ultrasound: shear wave speed propagation [3], the backscatter coefficient [4] and the spatial coherence [5–7].

The aim of this paper is to present our preliminary results of the spatial coherence method proposed in [5]. One main objective was to evaluate the possibility to reproduce the results in [5].The method is presented in the next section and then results obtained with this method from simulations and experimental acquisitions are presented and discussed.

2. Method

There are two ways to apprehend spatial coherence: coherence function and coherence imaging. They are based on the same transmission scheme with plane wave insonification. Only coherence function and its applications are detailed in this part.

2.1. Coherence function

The evaluation of the spatial coherence based on coherence factors calculated between the pre-beamformed signals obtained from focused ultrasound transmissions was initially proposed in [8]. However, the frame rate that can be achieved with focused transmission is too low to study *in vivo* the heart in three dimensions. In this case, ultrafast imaging based for example on plane wave imaging is more suitable. Plane wave imaging can reach several thousand volumes per second depending on the number of plane waves in transmission and the required depth used for the reconstruction. This is the reason why spatial coherence imaging was extended to plane wave imaging [5]. However, in order to calculate the coherence function it is necessary to have focused pre-beamformed RF signals. Therefore, a coherent plane wave compounding of the pre-beamformed signals is necessary as explained in [9] and detailed hereafter.

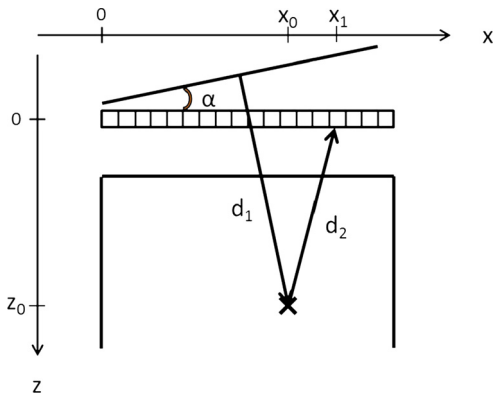

Fig. 1. Delay calculation for each point of the medium to each element on the probe. d_1 corresponds to the distance for the wave to reach the point-of-interest and d_2 corresponds to the distance for the wave to travel from the point-of-interest to the probe element in x_1.

In ultrasound plane wave imaging, a plane wave is transmitted in the medium and is scattered by the inhomogeneities of the medium. The echoes received by the probe elements are recorded and beamformed to produce an image [10]. These delays used to perform receive focusing are calculated for each point in the medium. For each plane wave a so-called low resolution image is beamformed and these images are coherently summed up to obtain the final image.

Spatial coherence calculation needs focused or rephased single element signals both in transmit and receive. In order to obtain these signals with plane wave transmissions, it is necessary to calculate the right delays for each point of the medium and each probe element. By choosing the right delays and after summation of the rephased signals from all plane waves, single element signals, written S, are obtained. This signals are equivalent to those obtained after receive focusing of the single element signals from focused transmissions. By applying delays on the pre-beamformed signals and summing them up, a synthetic transmit and receive focus is created. The travel time for the wave, with an α angle, to reach the scatterer (d_1 on Fig. 1) and travel back to the element in x_1 (d_2 on Fig. 1) were calculated for each spatial point [9].

$$d_1 = x_0 * \sin(\alpha) + z_0 * \cos(\alpha) \tag{1}$$

and

$$d_2 = \sqrt{z_0^2 + (x_0 - x_1)^2} \tag{2}$$

The focused or *rephased* signals written S_i where i corresponds to the probe element number, are used in the spatial coherence calculation for each spatial point. It consists of calculating a correlation factor between signals received by the different probe elements. Thus, for a point of the medium and after

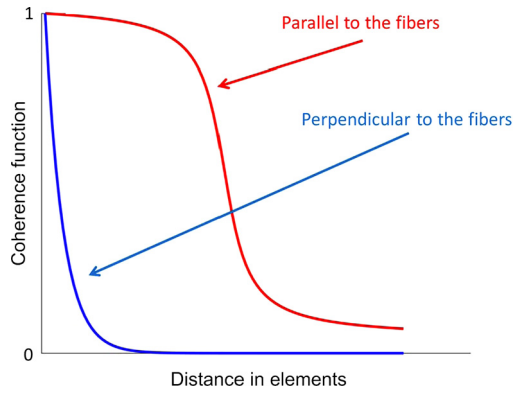

Fig. 2. Drawing representing the coherence function in two cases: the probe is parallel to the fibers (red) and the probe is perpendicular to the fibers (blue). (For interpretation of the references to color in this figure legend, the reader is referred to the web version of this article.)

delays application, pairs of signals S_i are compared starting with signals distant one element from each other and increasing the inter-element distance further and further as given in equation (3) to (5). In this way, the coherence function renders the coherence between the single elements signals as a function of their distance.

$$R(m) = \frac{N}{N-m} \sum_{i=1}^{N-m} \frac{c(i, i+m)}{\sqrt{c(i,i) * c(i+m, i+m)}} \tag{3}$$

with

$$c(i, j) = \sum_{T_1}^{T_2} \left(S_i(t) - \overline{S_i}\right)\left(S_j(t) - \overline{S_j}\right) \tag{4}$$

and

$$\overline{S_k} = \frac{1}{T_2 - T_1} \sum_{T_1}^{T_2} S_k(t) \tag{5}$$

where $[T_1; T_2]$ is the temporal window, N is the number of elements and m is the distance in number of elements between two elements compared [6,7].

Interestingly, when a medium is anisotropic, the coherence function decreases slowly. In contrary, when the medium is isotropic, the coherence function decreases faster [8]. In medium composed of fibers, the coherence function remains high when the probe is parallel to the fibers (anisotropic case) and decreases quickly when the probe is perpendicular to the fibers (isotropic case). Two typical coherence functions corresponding to isotropic and anisotropic tissue are represented in Fig. 2.

By calculating the coherence function for different probe angles around the probe axis, it is possible to find the direction for which the coherence function is the widest and has a value close to one [8]. This calculation can be repeated for every point in the medium. In this way, the local tissue orientation can be obtained for every spatial position. In the heart, this direction would correspond to the local cardiac fiber orientation.

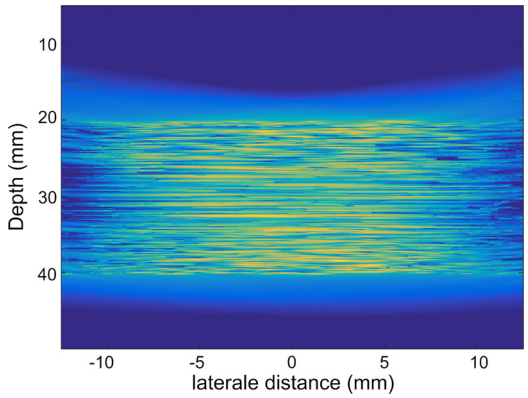

Fig. 3. Image obtained with CREANUIS software on fibers simulation. The fibers angle varying from $[-41°; 66°]$ for a thickness of 20 mm in depth.

2.2. Numerical simulation

In order to understand each step of the calculation, simulations were conducted using CREANUIS software to obtain control cases [11]. First, a medium with fibers oriented in one unique orientation has been modeled. Then, a more realistic medium was modeled with changes in fiber orientation as a function of depth. A realistic angle range of $[-41°; 66°]$ was used, as obtained in clinical situation [2]. The fibers were modeled by point scatterers placed in a same alignment. Each fiber was 10 mm long and consisted of 100 scatterers of same amplitude equal to one. 10,000 fibers were placed at random depths in a 20 mm thick medium. The considered volume size is $20 \times 40 \times 40$ mm^3 so the fibers density is 312.5 fibers per cm^3. The different parameters of the imaging systems were defined in order to correspond to the experimental setup used. The 128 elements linear array was used to generate 37 different plane waves from $-15°$ to $15°$. All 128 single element received signals were simulated. An example image obtained, with fibers angles changing as a function of depth, is displayed on Fig. 3.

2.3. Experimental acquisitions

In order to further study the method, experimental datasets were acquired using a Verasonics Vantage 256 system equipped with the L12-5mm probe (Philips) of 128 elements with a pitch of 195 µm. The probe was connected to a motor to enable its precise rotation (Owis DMT 65). Echoes were recorded by the probe with a 5° step. The ultrasound frequency was 7.8 MHz and the sampling frequency 31.2 MHz.

A phantom consisting of seven wires with angles varying between $[-45°; 45°]$ was designed and is displayed in Fig. 4. The diameter of each wire was 0.3 mm.

3. Results

3.1. Simulation

The coherence function was calculated on a simulation with fiber angles changing as a function of depth. In order to validate the methodology, the coherence function was calculated

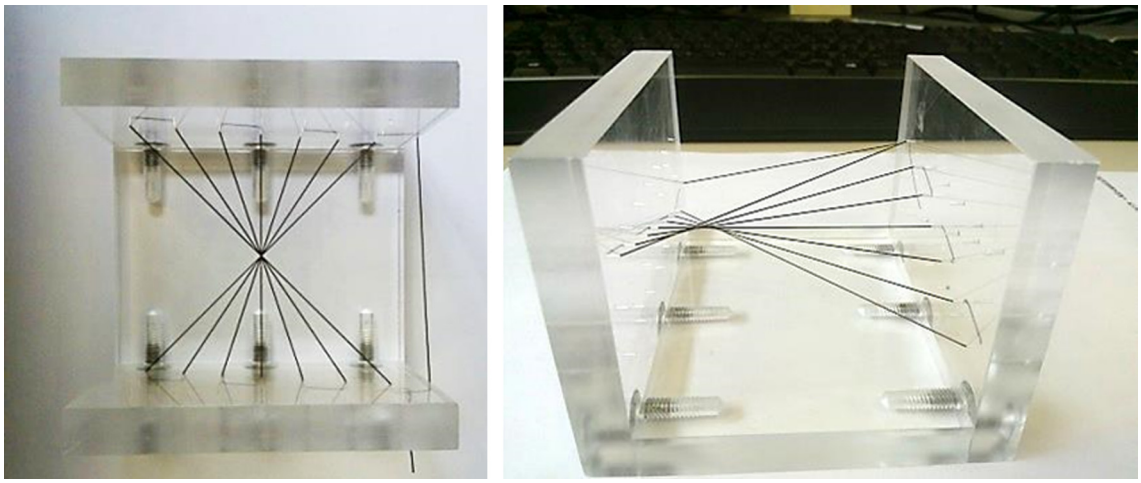

Fig. 4. Top and side views of the wire phantom consisting of 7 wires of diameter 0.3 mm distant of 10 mm between each other and with orientation varying between $[-45°; 45°]$.

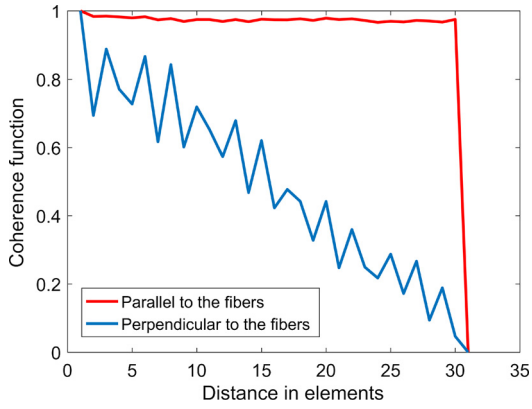

Fig. 5. Curve of coherence function in two cases: the probe is parallel to the fibers (red) and the probe is perpendicular to the fibers (blue). (For interpretation of the references to color in this figure legend, the reader is referred to the web version of this article.)

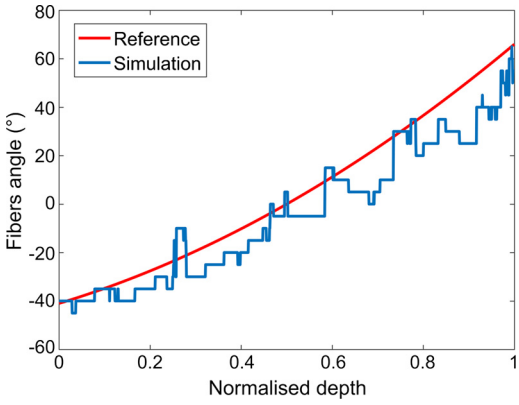

Fig. 6. Fibers angles as a function of normalized depth. The red line is the reference and the blue one corresponds to the angle obtained with the coherence function from the simulation data. (For interpretation of the references to color in this figure legend, the reader is referred to the web version of this article.)

in advance in two different situations in a specific point: the probe parallel to the fibers and perpendicular to the fibers. The functions obtained are plotted in Fig. 5. As expected, when the probe is parallel to the fibers, the coherence function stays constant and close to one. On the contrary, the coherence function decreases faster when the probe is perpendicular to the fibers.

In order to determine the local fiber orientation, this calculation was repeated for all probe angles. When the coherence function was the most constant and close to one, the corresponding probe direction was parallel to the fibers. On the contrary, the direction for which the curve decreased the fastest was identified as the direction for which the probe was perpendicular to the fibers. By calculating the coherence function for each probe angle, the fibers angle could be determined.

Next, this calculation was repeated for all depth in the medium. By calculating the coherence function for all probe angles and all depths, the fibers angle can be determined for all points in the medium along the probe rotation axis. Fig. 6 represents the fibers angle as a function of normalized depth obtained with this method along the central axis which is the same line for all probe angles.

To evaluate and quantify the proximity between the ground truth and evaluated angles, the root means square error (RMSE) was computed and is 11.2°.

3.2. Wires phantom

The coherence function corresponding to the positions of the wires in the phantom is represented in Fig. 7 which shows the coherence function on the first wire when the probe is parallel to the wire and when the probe is perpendicular to the wire. As expected, the coherence function decreases faster when the probe is perpendicular to the wire than when the probe is parallel to the wire.

Again the direction of the wire can be determined by finding the direction for which the coherence function is the closest to one and the widest. This process is repeated for each of the seven wires and the angle estimated for each wire is plotted in Fig. 8.

In this case, the RMSE was also computed to quantify the proximity to the ground truth. The RMSE obtained for these results is 16.5°.

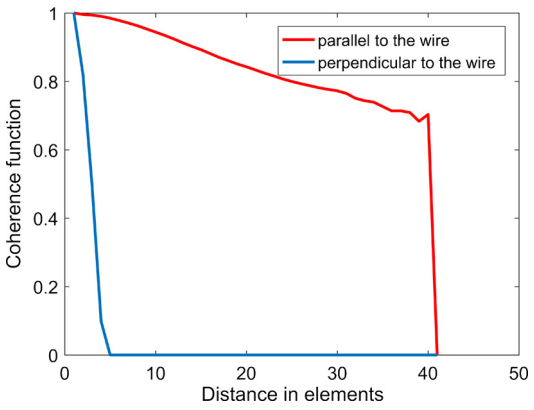

Fig. 7. Curve of the coherence function in two cases on the wires phantom: the probe is parallel to the wire (red) and the probe is perpendicular to the wire (blue) (For interpretation of the references to color in this figure legend, the reader is referred to the web version of this article.)

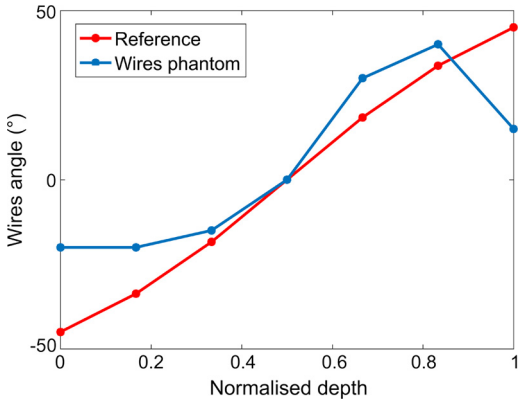

Fig. 8. Wires angle as a function of the normalized depth in the wire phantom. The red line is the reference and the blue one corresponds to the angle obtained with the coherence function from the experimental data. (For interpretation of the references to color in this figure legend, the reader is referred to the web version of this article.)

4. Discussion

The results obtained on simulations are in accordance with the theory for the spatial coherence curve. The estimated fibers angle as a function of the depth is close to the reference. These results confirm the efficiency of the studied method to recover the local orientation in a simulated medium. However, this is a simple case and there is neither noise nor artifacts as there usually is in experimental data. One can clearly see differences between the coherence function curves obtained with simulations and with experimental signals. This difference is explained in [8]. Actually, in theory, the curves are expected to decrease slowly. In practice, however, they decrease faster because of the noise present in experimental data. Simulation is an ideal case because there is neither noise nor artifacts, so the curves decrease in a very similar manner as the one expected in theory.

Furthermore, on experimental data, some wire angles were not determined with a high precision. This error is due to some misalignment between the rotation axis of the probe and the reference axis of the wire phantom. Indeed, this alignment is performed manually. This should definitely be improved in the future in order to have a more precise reference.

Moreover, there can be some approximation to determine wires angle because of the 5° probe angle step. In fact, the probe angle step is set at 5° leading to a maximum accuracy of 5° in the fiber's angle calculation.

In 2D, because of the probe rotation, this method cannot be used in a beating heart. So, this method was developed in 3D in [6]. In this case, it is no more necessary to rotate the probe. However, the impact of heart movement needs to be studied in order to adapt acquisition parameters like the number of transmission events.

The scale to detect the fibers angle could also be studied. For example, the different parameters such as ultrasound frequency, pulse size and probe size could be studied in order to see the impact on spatial resolution and its impact to detect fiber's angle on a very fine scale.

5. Conclusion

The spatial coherence was calculated on simulations and on a wires phantom. Simulations, which are a control cases, allow validating the method and each step of the calculation. Then, the wire phantom allows having simple experimental case.

This simple study enabled us to better understand the use of coherence functions to determine local tissue orientation. It is an interesting tool that we expect to further develop in our team and to compare with results obtained from diffusion MRI of the same media.

Conflict of interest statement

There is no conflict of interest in this article.

Acknowledgements

This work was supported by the LABEX PRIMES (ANR-11-LABX-0063) of Université de Lyon, within the program "Investissements d'Avenir" (ANR-11-IDEX-0007) operated by the French National Research Agency (ANR). The RF Verasonics generator was cofounded by the FEDER program, Saint-Etienne Metropole (SME) and Conseil General de la Loire (CG42) within the framework of the SonoCardio-Protection Project leaded by Pr Pierre Croisille.

References

[1] Wu M-T, Tsen W-Y, Su M-Y, Liu C-P, Chiu K-R, Wedeen V, et al. Diffusion tensor magnetic resonance imaging mapping the fiber architecture remodeling in human myocardium after infarction. Circulation 2016;114:1036–45.
[2] Lombaert H, Peyrat J-M, Croisille P, Rapacch S, Fanton L, Farida C, et al. Human aTLAS of the cardiac fiber architecture: study on a healthy population. IEEE Trans Med Imaging 2012;31(17).
[3] Lee W-N, Pernot M, Couade M, Messas E, Bruneval P, Bel A, et al. Mapping myocardial fiber orientation using echocardiography-based shear wave imaging. IEEE Trans Med Imaging 2012;31(13).
[4] Milne ML, Singh GK, Miller JG, Wallace KD, Holland MR. Toward 3-D echocardiographic determination of regional myofiber structure. Ultrasound Med Biol 2016;42(12):607–18.

[5] Papadacci C. Imagerie échographique ultrarapide du coeur et des artères chez l'homme: vers l'imagerie ultrarapide 3D et l'imagerie du tenseur de rétrodiffusion ultrasonore. Medical Physics. Université Paris-Diderot Paris 7; 2014.
[6] Papadacci C, Tanter M, Pernot M, Fink M. Ultrasound backscatter tensor imaging (BTI): analysis of the spatial coherence of ultrasonic speckle in anisotropic soft tissues. IEEE Trans Ultrason Ferroelectr Freq Control 2014;61(16).
[7] Papadacci C, Pinel V, Provost J, Villemain O, Bruneval P, Gennisson J-L, et al. Imaging the dynamics of cardiac fiber orientation in vivo using 3D ultrasound backscatter tensor imaging. Nat Sci Rep 2017.
[8] Fink M, Derode A. Spatial coherence of ultrasonic speckle in composites. IEEE Trans Ultrason Ferroelectr Freq Control 1993;40(16).
[9] Montaldo G, Tanter M, Bercoff J, Benech N, Fink M. Coherent plane-wave compounding for very high frame rate ultrasonography an transient elastography. IEEE Trans Ultrason Ferroelectr Freq Control 2009;56(13).
[10] Vray D, Brusseau E, Detti V, Varray F, Basarab A, Beuf O, et al. Ultrasound medical imaging. In: Medical imaging based on magnetic fields and ultrasounds. John Wiley & Sons, Inc.; 2014. p. 1–72.
[11] Varray F, Basset O, Tortoli P, Cachard C. CREANUIS: a nonlinear radio frequency ultrasound image simulator. Ultrasound Med Biol 2013;39:1915–24.